Evolution of a Gradient Microstructure in Direct Metal Laser Sintered AlSi10Mg

Amir Hadadzadeh, Babak Shalchi Amirkhiz, Brian Langelier, Jian Li and Mohsen Mohammadi

Abstract Unique and ultrafine microstructures are achieved through metal powder bed fusion additive manufacturing (AM) processes. However, a gradient in the microstructure through the height of tall-enough samples can be observed due to different cooling rates and heating–cooling cycles experienced by different locations. In the current study, a vertically built sample of AlSi10Mg with a rectangular cross section was manufactured through direct metal laser sintering (DMLS) process. The microstructure was studied at the bottom and top of the sample. From the bottom to the top of the DMLS-AlSi10Mg sample, fewer heating–cooling cycles were experienced by the material. Moreover, the cooling rate was different due to change of the thermal boundaries and cooling conditions. The microstructure of the DMLS-AlSi10Mg was analyzed using multi-scale characterization techniques including EBSD and APT. The microstructure characteristics were correlated to the solidification conditions experienced by the material.

Keywords Additive manufacturing · Direct metal laser sintering (DMLS) · EBSD · APT

A. Hadadzadeh (✉) · M. Mohammadi
Marine Additive Manufacturing Centre of Excellence (MAMCE), University of New Brunswick, Fredericton, NB E3B 5A1, Canada
e-mail: amir.hadadzadeh@unb.ca

A. Hadadzadeh · B. S. Amirkhiz · J. Li
CanmetMATERIALS, Natural Resources Canada, 183 Longwood Road South, Hamilton, ON L8P 0A5, Canada

B. Langelier
Canadian Centre for Electron Microscopy (CCEM), McMaster University, 1280 Main Street West, Hamilton, ON L8S 4M1, Canada

The Minerals, Metals & Materials Society (ed.), *TMS 2019 148th Annual Meeting & Exhibition Supplemental Proceedings*, The Minerals, Metals & Materials Series, https://doi.org/10.1007/978-3-030-05861-6_30

Introduction

Additive manufacturing (AM) as a breakthrough in advanced manufacturing is utilized to fabricate near-net shaped products directly from a CAD model using a feedstock material (powder or wire material) [1]. A high power beam is applied to selectively melt the feedstock to join the layers of material on top of each other [2] to create a part with a tailored microstructure [3]. Direct metal laser sintering (DMLS), also known as selective laser melting (SLM), is amongst the most commonly used AM processes due to its freedom of design, short production cycle, and potential cost savings [1, 4]. The cooling rate during DMLS process can reach 10^3–10^8 K/s, which leads to evolution of ultrafine, metastable and gradient microstructure [2] and production of high strength components [5]. DMLS of light metals, specifically aluminum alloys has been under extensive studies because of these advantages [6]. In addition, lightweight characteristics, high specific strength, and good corrosion properties of DMLS-AlSi10Mg have drawn the attention of engineers and designers in recent years [7]. Despite the evolution of very fine microstructure during DMLS of metallic materials, the components usually suffer from a columnar grain structure due to epitaxial grain growth [8], which causes anisotropy of microstructure, texture, and mechanical properties [9]. It was shown in a previous study that, by changing the building direction from vertical to horizontal, columnar-to-equiaxed transition (CET) occurred in DMLS-AlSi10Mg due to variation of thermal boundaries and G/V ratio (where G is thermal gradient in K/m and V is growth rate in m/s) [10]. CET also affected Si precipitates characteristics (size and coherency) and strengthening behavior of the alloy [11]. In addition to the build geometry, height of the sample can also change the thermal boundaries (specifically, cooling rates) and microstructure of the DMLS-AlSi10Mg [12]. This could be an opportunity to design components with a gradient microstructure.

Despite the observation of microstructural variation through the height of a sample, it is not clear how both micron (i.e. dendrites and grains) and submicron (i.e. Si precipitates) characteristics of DMLS-AlSi10Mg change. Therefore, the aim of this study was to analyze the microstructure evolution in a vertically built DMLS-AlSi10Mg sample. A rectangular cuboid sample with dimensions of 10 mm × 20 mm × 40 mm was vertically built using DMLS process. The microstructure of the sample was analyzed using electron backscatter diffraction (EBSD) and atom probe tomography (APT) techniques at various heights to understand how micron and submicron characteristics of the sample evolved during the process.

Experimental Procedure

A rectangular cuboid sample with dimensions of 10 mm × 20 mm × 40 mm was vertically built through DMLS process using an EOS M290 machine, as shown schematically in Fig. 1. The machine was equipped with a building plate of 250 mm

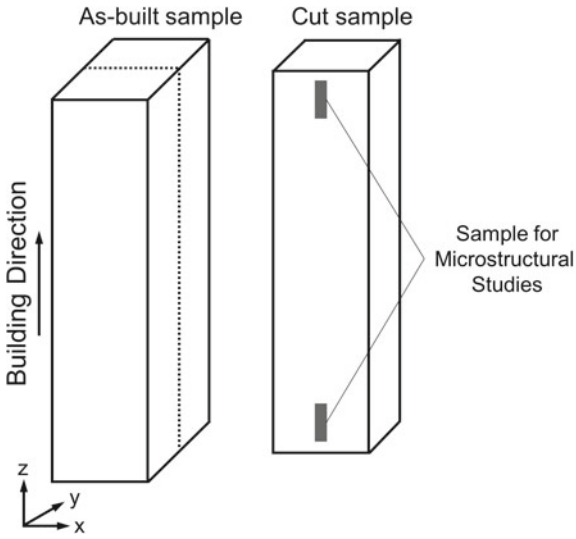

Fig. 1 Schematic of DMLS-AlSi10Mg sample along with the samples used for microstructural studies

× 250 mm × 325 mm, a 400 W Yb-fiber laser (maximum capability), and a laser beam with spot size of 100 μm. The process was conducted in an argon atmosphere with maximum 0.1% oxygen content. The sample was fabricated using AlSi10Mg virgin powder with an average particle size of 9 ± 7 μm and a chemical composition of Al-10 wt% Si-0.33 wt% Mg-0.55 wt% Fe. The process parameters used for DMLS of AlSi10Mg were recommended by EOS GmbH to obtain the least porosity in the core of the sample and reported elsewhere [10].

Microstructure of the as-built sample was analyzed using EBSD at the mid-plane position along the centre line of the sample, as shown in Fig. 1. EBSD scans were conducted over an area of 400 μm × 800 μm with a step size of 0.3 μm in a field emission gun scanning electron microscope (FEG-SEM FEI Nova NanoSEM-650) equipped with a Hikari EBSD system.

APT analyses were conducted along the same locations of EBSD analyses, using a local electrode atom probe (LEAP) 4000X HR (CAMECA Scientific Instruments, Madison, WI), equipped with a reflectron. Measurements were performed in ultra-high vacuum ($<4 \times 10^{-11}$ Torr) at a temperature of about 60 K. Field evaporation from the samples were promoted using ultraviolet (UV) laser pulses ($\lambda = 355$ nm) with a pulse energy of 60 pJ and a pulse rate of 125–250 kHz. The target detection rate (controlled by varying the DC voltage applied to the sample) was 5 ions per 1000 pulses. Reconstruction of the acquired data was conducted using the integrated visualization and analysis software package (IVAS) v3.8 (CAMECA Scientific Instruments, Madison, WI). Sample preparation for APT was done using an NVision 40 focused ion beam (FIB) instrument (Carl Zeiss, Germany) and established lift-out techniques, with details described elsewhere [13]. Final cleaning of the specimen tips was done at a low voltage (5 kV) to minimize Ga implantation and damage to the samples.

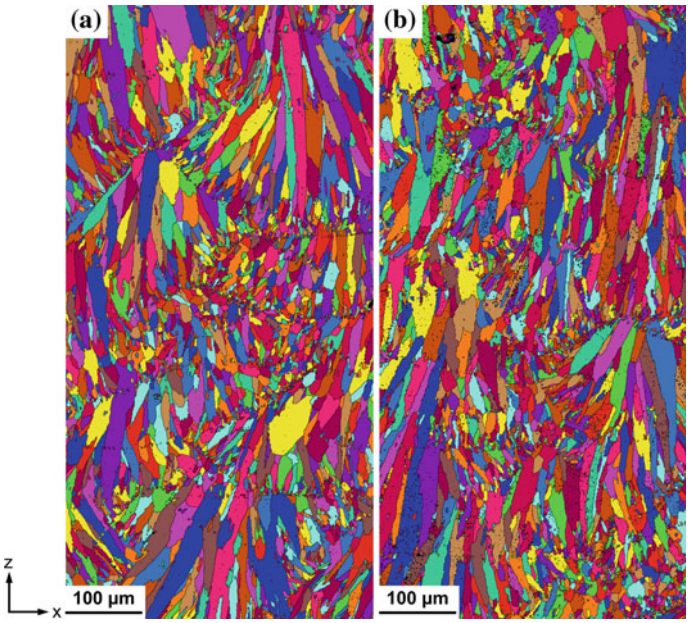

Fig. 2 EBSD unique color grain maps of **a** bottom and **b** top of the sample

Results and Discussion

Figure 2 shows the typical EBSD map of bottom and top of the sample. The microstructure of the sample consisted of overlapped melt pools as a result of layer-on-layer deposition [11]. A columnar microstructure is developed inside the melt pools due to epitaxial growth, while the pool boundaries are featured by equiaxed grains. It was shown previously that each elongated grain consisted of several α-Al dendrites bounded by eutectic Si walls [10].

To better interpret the microstructural features of the alloy and the differences between bottom and top of the sample, grains were analyzed considering the grain shape aspect ratio (ϕ), which represents the ratio between the minor axis (L_2) and major axis (L_1) of each individual grain ($\phi = L_2/L_1$). The minor and major axes of each grain were evaluated by fitting an ellipse to each grain [10]. Figure 3a shows the area fraction of grains with different grain shape aspect ratios, at the bottom and top of the sample. Columnar and equiaxed grains were defined with $\phi \leq 0.33$ and $\phi > 0.33$, respectively [14]. Referring to Fig. 3a, 76–78% of grains are columnar in both bottom and top specimens. Moreover, the grain size area (in μm^2) of the DMLS-AlSi10Mg was very consistent at the bottom and top of the samples, as shown in Fig. 3b. Such a consistency in the grains characteristics seems to be a result of similar solidification conditions along the height of the sample.

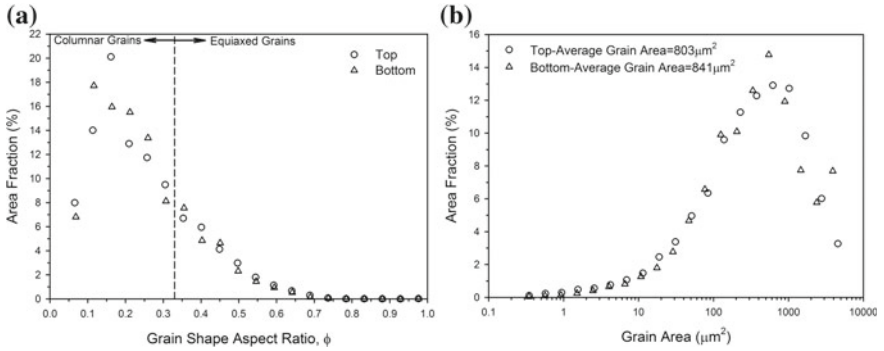

Fig. 3 **a** Grain shape aspect ratio and **b** grain size area at bottom and top of the sample

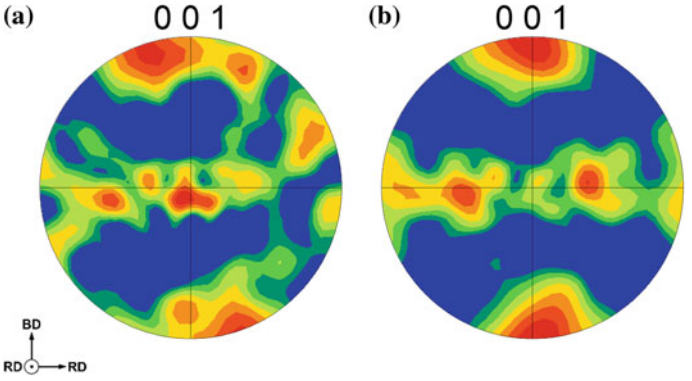

Fig. 4 (001) EBSD pole figures of **a** bottom and **b** top of DMLS-AlSi10Mg. Note: BD and RD represent building direction and radial direction, respectively

It was shown in a previous study [10] that during DMLS of AlSi10Mg the constitutional undercooling which determines the solidification morphology (equiaxed or columnar) is dependent on G/V ratio. In addition, as the ψ-angle (the angle between the nominal growth rate and $\langle hkl \rangle$ direction of the growing dendrites) decreased, G/V ratio increased, and a lower constitutional undercooling is obtained which led to the formation of a columnar structure. Since <001> direction is the major dendritic growth (easy-growing) direction in FCC metals and alloys [15], <001> texture represents the solidification mode in DMLS-AlSi10Mg [10]. Figure 4 shows the (001) pole figures at the bottom and top of DMLS-AlSi10Mg sample, obtained from EBSD analyses. As seen, in both locations, {001} fibre texture evolved as a result of $<001>$ // z (building direction) growth. The consistency of ψ-angle at the bottom and top of the sample resulted in similar constitutional undercoolings and evolution of similar grain morphologies.

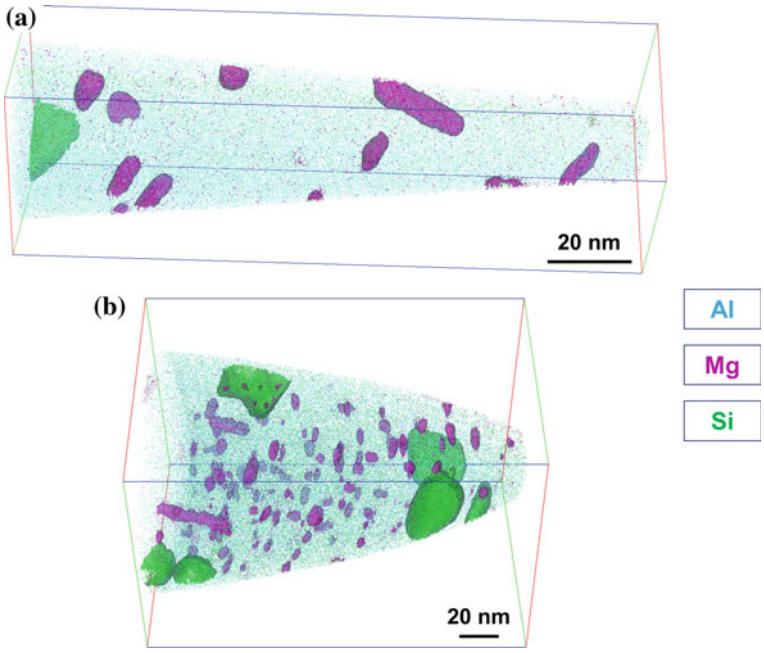

Fig. 5 3D APT atom maps showing the distributions of Al, Mg and Si elements inside the melt pools of **a** bottom and **b** top specimens. Precipitates are highlighted by iso-concentration surfaces for 3 at.% Mg or 3 at.% Si

Despite the similarities in the microstructural characteristics of bottom and top of DMLS-AlSi10Mg, submicron characteristics of these two locations were different, as shown in Fig. 5. While both Si and MgSi precipitates developed on the top of the sample (Fig. 5b), only MgSi precipitates evolved in the bottom of the sample (Fig. 5a). Moreover, by moving from the top to the bottom of DMLS-AlSi10Mg, fine and dispersed MgSi precipitates are changed to large, needle-shaped ones. The absence of Si precipitates in the bottom of the sample is a result of various heating cycles experienced by the material, which led to dissolution of Si precipitates [12]. On the other hand, MgSi precipitates grew due to diffusion of Mg in the aluminum matrix. It was shown before that Si precipitates play an important role on the strength of DMLS-AlSi10Mg [5, 11]; therefore, their absence can compromise the strength of the alloy. On the other hand, variation of the characteristics of MgSi precipitates can affect the strength of DMLS-AlSi10Mg. Hence, it is essential to investigate the effect of submicron characteristics on the strength of the alloy in detail.

Conclusions

In the current study, the microstructure of a vertically built DMLS-AlSi0 Mg sample was analyzed at two extreme locations; bottom and top of the sample using EBSD and APT techniques to investigate the evolution of micron and submicron characteristics of the alloy during the DMLS process. The microstructure of the sample at the bottom and top was consistent and comprised of columnar grains developed along the building direction. The majority of the grains (76–78%) were columnar in both locations and the grain area was similar. Evolution of {001} fibre texture as a result of <001> // z (building direction) growth was the main reason for columnar structure development, considering the fundamentals of solidification and constitutional undercooling. Despite the similarities in the microstructural characteristics of bottom and top of DMLS-AlSi10Mg, submicron characteristics of these two locations were different. While both Si and MgSi precipitates developed on the top of the sample, only MgSi precipitates evolved in the bottom of DMLS-AlSi10Mg. Moreover, by moving from the top to the bottom of DMLS-AlSi10Mg, fine and dispersed MgSi precipitates are transformed to large, needle-shaped ones. Differences in submicron characteristics can potentially affect the strength of DMLS-AlSi10Mg.

Acknowledgements The authors would like to acknowledge Natural Sciences and Engineering Research Council of Canada (NSERC) project number RGPIN-2016-04221 and New Brunswick Innovation Foundation project number (NBIF)-RIF2017-071 for the financial support of this work. The authors would also like to acknowledge Dr. Mark Kozdras at CanmetMATERIALS for facilitating the research. APT analysis was carried out at the Canadian Centre for Electron Microscopy (CCEM), a facility supported by McMaster University, the Canada Foundation for Innovation under the Major Science Initiative program and NSERC.

References

1. Gu DD, Meiners W, Wissenbach K, Poprawe R (2012) Laser additive manufacturing of metallic components: materials, processes and mechanisms. Int Mat Rev 57:133–164
2. Herzog D, Seyda V, Wycisk E, Emmelmann C (2016) Additive manufacturing of metals. Acta Mater 117:371–392
3. DebRoy T, Wei HL, Zuback JS, Mukherjee T, Elmer JW, Milewski JO, Beese AM, Wilson-Heid A, De A, Zhang W (2018) Additive manufacturing of metallic components—process, structure and properties. Prog Mater Sci 92:112–224
4. Martin JH, Yahata BD, Hundley JM, Mayer JA, Schaedler TA, Pollock TM (2017) 3D printing of high-strength aluminium alloys. Nature 549:365–369
5. Hadadzadeh A, Baxter C, Shalchi Amirkhiz B, Mohammadi M (2018) Strengthening mechanisms in direct metal laser sintered AlSi10Mg: comparison between virgin and recycled powders. Addit Manuf 23:108–120
6. Olakanmi EO, Cochrane RF, Dalgarno KW (2015) A review on selective laser sintering/melting (SLS/SLM) of aluminium alloy powders: processing, microstructure, and properties. Prog Mater Sci 74:401–477
7. Read N, Wang W, Essa K, Attallah MM (2015) Selective laser melting of AlSi10Mg alloy: process optimisation and mechanical properties development. Mater Des 65:417–424

8. Basak A, Das S (2016) Epitaxy and microstructure evolution in metal additive manufacturing. Annu Rev Mater Res 46:125–149
9. Kok Y, Tan XP, Wang P, Nai MLS, Loh NH, Liu E, Tor SB (2018) Anisotropy and heterogeneity of microstructure and mechanical properties in metal additive manufacturing: a critical review. Mater Des 139:565–586
10. Hadadzadeh A, Amirkhiz BS, Li J, Mohammadi M (2018) Columnar to equiaxed transition during direct metal laser sintering of AlSi10Mg alloy: effect of building direction. Addit Manuf 23:121–131
11. Hadadzadeh A, Amirkhiz BS, Odeshi A, Mohammadi M (2018) Dynamic loading of direct metal laser sintered AlSi10Mg alloy: strengthening behavior in different building directions. Mater Des 159:201–211
12. Liu YJ, Liu Z, Jiang Y, Wang GW, Yang Y, Zhang LC (2018) Gradient in microstructure and mechanical property of selective laser melted AlSi10Mg. J Alloy Compd 735:1414–1421
13. Persaud SY, Smith JM, Langelier B, Capell B, Wright MD (2018) An atom probe tomography study of Pb-caustic SCC in alloy 800. Corros Sci 140:159–167
14. Yang KV, Shi Y, Palm F, Wu X, Rometsch P (2018) Columnar to equiaxed transition in Al-Mg(-Sc)-Zr alloys produced by selective laser melting. Scr Mater 145:113–117
15. Gaumann M, Bezencon C, Canalis P, Kurz W (2001) Single-crystal laser deposition of superalloys: processing–microstructure maps. Acta Mater 49:1051–1062